HHS Public Access
Author manuscript
Cell Metab. Author manuscript; available in PMC 2022 March 02.

Published in final edited form as:
Cell Metab. 2021 March 02; 33(3): 499–512.e6. doi:10.1016/j.cmet.2021.01.018.

Creatine mediated crosstalk between adipocytes and cancer cells regulates obesity-driven breast cancer

Olivia A. Maguire[1,2,*], **Sarah E. Ackerman**[1,4,*], **Sarah K. Szwed**[1,2], **Aarthi V. Maganti**[1], **François Marchildon**[1], **Xiaojing Huang**[3], **Daniel J. Kramer**[1,2], **Adriana Rosas-Villegas**[1], **Rebecca G. Gelfer**[2], **Lauren E. Turner**[1], **Victor Ceballos**[1], **Asal Hejazi**[1], **Bozena Samborska**[5,6], **Janane F. Rahbani**[5,6], **Christien B. Dykstra**[5,6], **Matthew G. Annis**[5], **Ji-Dung Luo**[7], **Thomas S. Carroll**[7], **Caroline S. Jiang**[8], **Andrew J. Dannenberg**[9], **Peter M. Siegel**[5,6], **Sarah A. Tersey**[10], **Raghavendra G. Mirmira**[10], **Lawrence Kazak**[5,6], **Paul Cohen**[1,11,12]

[1]Laboratory of Molecular Metabolism, The Rockefeller University, New York, NY 10065, USA

[2]Weill Cornell/Rockefeller/Sloan Kettering Tri-institutional MD-PhD Program, New York NY 10065, USA

[3]Memorial Sloan Kettering Cancer Center, New York, NY 10065, USA

[4]AAAS Science and Technology Policy Fellow in the Office of Global Health, Health Workforce Branch, U.S. Agency for International Development, Washington, D.C. 20547, USA**

[5]Goodman Cancer Research Centre, McGill University, Montreal, QC, H3A 1A3, Canada

[6]Department of Biochemistry, McGill University, Montreal, Quebec H3G1Y6, Canada

[7]Bioinformatics Resource Center, The Rockefeller University, New York, NY 10065, USA

[8]Rockefeller University Hospital, The Rockefeller University, New York, NY 10065, USA

[9]Department of Medicine, Weill Cornell Medical College, New York, NY 10065, USA

[10]Department of Medicine, The University of Chicago, Chicago, IL 60637, USA

[12]Lead contact

---

[11] Corresponding author: pcohen@rockefeller.edu.

[*]These authors contributed equally to this work.

[**]The contents in this manuscript are those of the authors and do not necessarily reflect the view of the U.S. President's Emergency Plan for AIDS Relief, the U.S. Agency for International Development or the U.S. Government.

Author contributions: P.C. conceived of the project and supervised the research. P.C, O.A.M, and S.E.A designed the experiments. O.A.M., S.E.A., S.K.S., A.V.M., F.M., X.H., D.J.K., A.R., R.G.G., L.T., V.C., A.H., B.S., J.F.R., C.D, and M.G.A. performed, analyzed, and/or assisted with experiments. O.A.M, S.E.A., J.L., T.S.C., and C.S.J. analyzed the data. O.A.M, S.E.A., and P.C. wrote the manuscript with contributions from all authors. A.J.D., P.M.S., S.A.T., R.G.M, and L.K. provided reagents and intellectual input.

Publisher's Disclaimer: This is a PDF file of an unedited manuscript that has been accepted for publication. As a service to our customers we are providing this early version of the manuscript. The manuscript will undergo copyediting, typesetting, and review of the resulting proof before it is published in its final form. Please note that during the production process errors may be discovered which could affect the content, and all legal disclaimers that apply to the journal pertain.

Inclusion and diversity
One or more of the authors of this paper self-identifies as an underrepresented ethnic minority in science. One or more of the authors of this paper self-identifies as a member of the LGBTQ+ community. One of more of the authors of this paper received support from a program designed to increase minority representation in science.

Declaration of interests:
The authors declare no competing interests.

Summary:

Obesity is a major risk factor for adverse outcomes in breast cancer; however, the underlying molecular mechanisms have not been elucidated. To investigate the role of crosstalk between mammary adipocytes and neoplastic cells in the tumor microenvironment (TME), we performed transcriptomic analysis of cancer cells and adjacent adipose tissue in a murine model of obesity-accelerated breast cancer and identified glycine amidinotransferase (Gatm) in adipocytes and Acsbg1 in cancer cells as required for obesity-driven tumor progression. Gatm is the rate-limiting enzyme in creatine biosynthesis, and deletion in adipocytes attenuated obesity-driven tumor growth. Similarly, genetic inhibition of creatine import into cancer cells reduced tumor growth in obesity. In parallel, breast cancer cells in obese animals upregulated the fatty acyl-CoA synthetase, Acsbg1, to promote creatine-dependent tumor progression. These findings reveal key nodes in the crosstalk between adipocytes and cancer cells in the TME necessary for obesity-driven breast cancer progression.

eTOC summary

Obesity is a major risk factor for adverse outcomes in breast cancer. Maguire, Ackerman et al. reveal Gatm and Acsbg1 as molecular regulators of obesity-driven breast cancer progression. They further show that in obesity creatine is a key metabolite in the crosstalk between adipocytes and breast tumors.

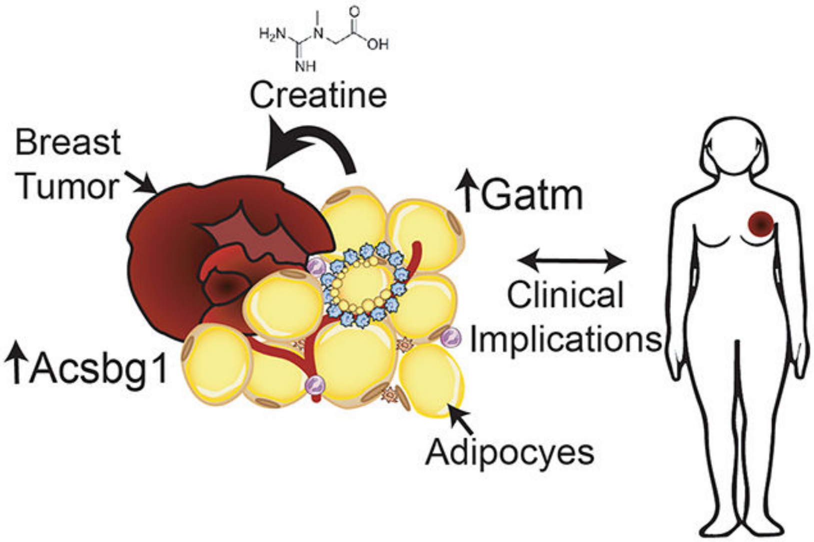

Keywords

breast cancer; obesity; creatine; Gatm; Acsbg1; hypoxia

Introduction:

Obesity is a risk factor for several types of cancer and is quickly overtaking tobacco as the leading preventable cause of cancer, with excess body weight implicated in 15-20% of total cancer-related mortality (Ligibel et al., 2014; Global BMI Mortality Collaboration, 2016).

The prevalence of overweight and obesity has increased dramatically in the past few decades, affecting more than 70% of adults in the United States and nearly 2 billion worldwide (Hales et al., 2017). Consequently, there is an urgent need to identify molecular mechanisms underlying obesity-driven cancer.

Among obesity-associated cancers in women, breast cancer is a leading cause of mortality. Obese women with a body mass index (BMI) greater than 40, regardless of menopausal or hormone receptor status, are at increased risk for disease recurrence (Calle et al., 2003; Reeves et al., 2007; Renehan et al., 2008; Bhaskaran et al., 2014) and have a 2.12-fold increased risk of death relative to normal weight women (Bastarrachea et al., 1994). Triplenegative breast cancer (TNBC) is a particularly aggressive subtype of the disease with worse outcomes and fewer treatment options, with obese pre-menopausal women at increased risk for its development.

The molecular mechanisms underlying the strong association between obesity and poor breast cancer outcomes are not well understood. In addition to systemic changes in hormonal signaling, obesity results in local changes to the adipose-dominated mammary TME that may contribute to cancer progression (Park, Euhus and Scherer, 2011; Park and Scherer, 2012; Quail and Dannenberg, 2019; Perry and Shulman, 2020). We sought to investigate whether coordinated changes in the cellular and metabolic phenotypes of mammary adipocytes and breast cancer cells are responsible for accelerated tumor progression in obesity.

Using a murine model of obesity-accelerated TNBC, we performed transcriptomic analyses of both the neoplastic cells and the adjacent mammary adipose tissue to identify pathways linking obesity and breast cancer progression. We identified a role for adipocyte-specific creatine biosynthesis in facilitating obesity-accelerated tumor progression. This pathway was complemented by upregulation of the acyl-coA synthetase, *Acsbg1*, in cancer cells, a phenomenon that was obesity-dependent and required intact creatine transport. Gene expression analysis from two large human cohorts revealed that high expression of *SLC6A8* and *ACSBG1* were significantly associated with worse tumor grade and that high expression of *SLC6A8* was associated with reduced disease free survival in triple negative breast cancer, suggesting a role for these pathways in the pathogenesis of the human disease (Toro et al., 2016). The data presented here define a hitherto undescribed pathway centered on creatine metabolism that drives communication between adipocytes and cancer cells in the TME in the specific context of obesity.

Results:

Diet-induced obesity promotes breast tumor progression

To study obesity-accelerated breast cancer, we used a diet-induced model of obesity (DIO) in wild-type C57Bl/6J (B6) animals. After 12 weeks on 60% high-fat diet (HFD), female B6 mice weighed 33% more ($p<0.0001$) than lean, chow fed controls, which was due to increased fat mass (Fig. 1, A and B). As expected, blood glucose and insulin were 1.4-fold ($p<0.0001$) and 3-fold ($p=0.005$) greater respectively, in obese mice compared to lean controls, with no differences between tumor-bearing and non-tumor-bearing animals (Fig. S1, A and B).

We used the B6 syngeneic functionally triple-negative E0771 (Johnstone et al., 2015) orthotopic breast cancer model to create rapidly growing tumors *in vivo* for characterization in lean and obese animals. After 9 weeks on a HFD or chow diet, female mice had E0771 cells implanted into the fourth mammary pad, and the resulting tumor volumes were measured longitudinally. E0771 tumors in obese mice were significantly larger than tumors in lean mice at matched time points (Fig. 1C). At the pre-specified endpoint of 20 days, tumors from obese mice were 5.5-fold larger (p=0.0001) in volume than tumors from lean controls (Fig. 1C, Fig S1, C and D). Obese tumors were significantly more proliferative than lean tumors, as measured by EdU incorporation (Fig 1D), while we detected no difference in apoptosis, as quantified by cleaved caspase 3 positivity (Fig 1E, Fig S1E). Furthermore, obese tumors were more hypoxic than lean tumors, as measured by HIF1-α protein levels, consistent with increased tumor size (Fig 1F).

To investigate if dietary components caused accelerated tumor growth, we used a pair-feeding regimen and demonstrated that *ad libitum* HFD fed animals gained 50% more weight than *ad libitum* low fat diet (LFD) fed mice, largely due to increased fat mass (4.4-fold) (Fig. S1, F and G). Notably, HFD *ad libitum* fed animals also gained significantly more weight and fat mass (2.2-fold) than HFD fed animals calorically matched to the LFD group (HFD-pair fed) (Fig. S1, F and G). We repeated the E0771 orthotopic experiment above in these groups of mice. Tumors in HFD mice showed accelerated progression compared to tumors in LFD or HFD pair-fed mice (p=0.001), while there was no difference in tumor progression between LFD and HFD pair fed groups (Fig. S1H). These data indicate that increased caloric consumption and concomitant obesity are responsible for the increased tumor progression we observe in this model of obesity accelerated breast cancer progression.

Transcriptomic analysis of peritumoral adipose tissue

We hypothesized that molecular changes in adipose tissue immediately adjacent to cancer cells may play a role in obesity-accelerated tumor growth. Therefore, we used RNA sequencing of peritumoral (immediately surrounding the tumor) and contralateral mammary fat to identify gene expression changes unique to adipose tissue in the obese TME (Fig. 2A). We compared the following six groups: lean peritumoral, lean contralateral, obese peritumoral, obese contralateral, lean non-tumor bearing, and obese non-tumor bearing. Principal component analysis (PCA) illustrated that the groups clustered by obesity status (PC 1) and the presence of a tumor (PC 2), demonstrating that the tumor has a profound effect on the molecular phenotype of surrounding adipose tissue (Fig. S2A). Notably, peritumoral adipose tissue from obese tumor-bearing mice was most distinct from the other groups (Fig. S2A), consistent with substantial and selective gene expression changes in this microenvironment.

The unique gene signature of obese peritumoral adipose tissue suggests that crosstalk between this tissue and nearby proliferating cancer cells is a key driver of overall tumor growth. As altered metabolism is increasingly recognized as a hallmark of tumorigenesis and progression (Hanahan and Weinberg, 2011), we performed KEGG pathway mapping to identify putative metabolic pathways differentially regulated between peritumoral and contralateral adipose tissue in obesity (Luo et al., 2009) (Fig. 2B). Many of the pathways identified have been implicated in tumorigenesis (e.g. purine and pyrimidine metabolism), especially in cell autonomous contexts, but few have been studied in the context of interactions between cancer cells and surrounding stromal cells, including adipose. Of the pathways identified, we hypothesized that arginine and proline metabolism could be relevant to TME crosstalk given its connections to paracrine signals such as nitric oxide and extracellular matrix composition (Phang et al., 2015; Jr, 2016). Among the top dysregulated genes within the arginine and proline metabolism pathway was glycine amidinotransferase (*Gatm*), the rate-limiting enzyme in creatine biosynthesis (Fig. 2C). *Gatm* was upregulated 4.7-fold (p=0.007) in obese peritumoral adipose compared to obese contralateral adipose (Fig. 2D). *Gatm* was also slightly upregulated, 2.9-fold, in lean peritumoral adipose compared to contralateral fat, but this did not reach statistical significance. Importantly, there was no difference in *Gatm* expression between lean and obese contralateral fat (Fig. 2D) or between lean and obese adipose in non-tumor bearing mice (data not shown), indicating that upregulation of *Gatm* is dependent on both obesity and the presence of cancer cells in the microenvironment. There was no difference in *Gatm* expression in tumors from lean or obese animals by RT-qPCR, and peritumoral adipose tissue displayed *Gatm* expression levels similar to that in tumors (Fig. S2B).

Mammary adipose tissue contains a variety of cell types. To investigate if *Gatm* upregulation occurred in peritumoral adipocytes or in resident non-adipose cell types within the tissue, we generated adipocyte-specific Rosa26$^{\text{fsTRAP}}$ (Adipo-TRAP) mice (Zhou et al., 2013). Adipo-TRAP mice express GFP-tagged ribosomes under the control of the adiponectin promoter. We then used lean or obese female Adipo-TRAP animals in an E0771 orthotopic experiment and the translating ribosome affinity purification (TRAP) technique to isolate ribosome-bound mRNA in an adipocyte-specific manner. We quantified *Gatm* mRNA levels by RT-qPCR and found an 11.5-fold increase (p=0.04) in obese peritumoral adipocytes compared to bulk peritumoral adipose tissue (input) (Fig. 2F), yet interestingly *Gatm* mRNA showed no significant enrichment in obese contralateral adipocytes. Additionally, *Gatm* mRNA was not enriched in adipocytes of lean tumor bearing mice (Fig. 2E). Finally, we used liquid chromatography coupled to mass spectrometry (LC/MS) to measure creatine and phosphocreatine levels in bulk tumors from lean and obese mice at an early time point (D13), before tumors diverged in size (Fig. S2 C and D). We found there was a significant increase in creatine (p=0.0392) and a trend towards increased phosphocreatine (p=0.1982) in tumors from obese compared to lean mice (Fig. 2 G and H). Collectively, these data demonstrate that increased *Gatm* expression in adipocytes is highly context dependent, specific to both obesity and localization in the peritumoral environment, and that tumors in obese mice contain higher levels of creatine and phosphocreatine.

Obesity-accelerated tumor growth is dependent on adipocyte Gatm

To investigate the role of endogenous creatine synthesis in adipocytes, we employed a murine strain with a targeted adipose-selective deletion of *Gatm* (Adipo-Gatm KO mice) (Kazak et al., 2017). We confirmed tissue-specific *Gatm* knockout by RT-qPCR of the mature adipocyte fraction of mammary adipose tissue and in cultured, differentiated adipocytes from the stromal vascular fraction (Fig. 2, I and J). Female Adipo-*Gatm* KO and littermate control mice (*Gatm*$^{fl/fl}$) were placed on either chow or HFD diet for 9 weeks. When these Adipo-*Gatm* KO mice are fed HFD at thermoneutrality (28-30°C), they become more obese than controls (Kazak et al., 2017), thus confounding their usage here. We therefore fed mice HFD at room temperature, where the classical thermogenic UCP1 pathway is expected to be more active (Kazak et al., 2017) and may suppress weight differences between the genotypes. Obese Adipo-*Gatm* KO and littermate control mice weighed 60% more than lean mice of either genotype ($p<0.0001$) (Fig. 2K). While obese Adipo-*Gatm* KO mice weighed slightly less than obese control mice (Fig. 2K), there was no difference in fat mass, with both groups accumulating 6-fold more fat mass than lean mice of either genotype ($p<0.0001$) (Fig. 2L) There was no difference in serum insulin or glucose among the groups (Fig. S2 E and F).

Using lean or obese female Adipo-*Gatm* KO or control mice in an orthotopic E0771 experiment, we found that tumors in obese control mice were on average 3.6-fold greater in volume compared to tumors in lean control mice, consistent with our previous results. However, tumors in obese Adipo-*Gatm* KO mice showed markedly decreased progression compared to tumors in obese control mice (Fig. 2M). At endpoint, tumors in obese Adipo-Gatm KO mice were 42% ($p=0.0005$) smaller than tumors in obese control mice (Fig. 2M). Although these animals had slightly decreased body weight, regression analysis revealed that the difference in body weight between groups was not a predictor of the difference in tumor volume ($p=0.1392$ with mixed effects model for repeated measures). Importantly, there was no difference in tumor volume between lean Adipo-*Gatm* KO and littermate control mice (Fig. 2M), illustrating that *Gatm* expression in adipocytes plays a unique role in promoting breast tumor progression in the context of obesity.

To examine how *Gatm* expression in adipocytes affects long-term breast cancer survival, we repeated the orthotopic E0771 experiment in lean or obese Adipo-Gatm KO or control female animals and monitored survival. Obese Adipo-*Gatm* KO and littermate control mice weighed 80% more than lean mice ($p<0.0001$), with no difference in body weight between the obese groups (Fig. S2G). Strikingly, obese Adipo-*Gatm* KO mice showed a significant survival benefit compared to littermate controls (Fig. S2H), while there was no difference between lean Adipo-*Gatm* KO and control mice.

To test whether exogenous creatine supplementation augments tumor progression, we fed animals control LFD or HFD or these same diets supplemented with creatine. Animals fed creatine supplemented diets were not significantly different in body weight than animals fed control diets (Fig. S3A). We then performed an orthotopic E0771 experiment using these four groups of animals and found no difference in tumor volume between animals fed control LFD or LFD supplemented with creatine. Similarly, there was no difference in tumor volume between animals fed control HFD or HFD supplemented with creatine (Fig. S3B). These data suggest that creatine from the TME, but not exogenous creatine from the diet, plays an important role in promoting obesity-accelerated tumor growth.

To confirm that exogenous creatine is transported into E0771 cancer cells, we incubated cells with labeled m+3 deuterated creatine (D-3 creatine) and traced its fate using LC/MS.

D-3 creatine was taken up by E0771 cells (Fig. S3 C–E), resulting in an increase in the labeled m+3 isotopologue of phosphocreatine (Fig. S3 F–H), suggesting that exogenous creatine is converted into phosphocreatine in E0771 cancer cells. We used a short hairpin to silence the creatine transporter, solute carrier family 6 member 8 (*Slc6a8*) and found that *Slc6a8* mRNA was reduced by 91% (p=0.002), and SLC6A8 protein was markedly reduced in *Slc6a8* KD compared to control cells (Fig. 3, A and B). When cultured with labeled creatine, *Slc6a8* KD cells accumulated significantly less labeled creatine and phosphocreatine than control cells (Fig. S3 C-H). Therefore, creatine uptake into E0771 cells is dependent on *Slc6a8.*

In addition to creatine biosynthesis, arginine can be diverted to polyamine synthesis through the production of ornithine (Fig. 2C). The rate limiting step in polyamine synthesis is the conversion of ornithine to putrescine by ornithine decarboxylase 1 (ODC1). To investigate if polyamine synthesis supports obesity-accelerated tumor growth, we generated adipocyte-specific *Odc1* knock-out mice (Adipo-*Odc1* KO). We confirmed that *Odc1* was deleted in adipose of Adipo-*Odc1* KO animals by RT-qPCR of mammary adipose tissue (Fig. S3I). Adipo-*Odc1* KO animals and littermate controls on HFD weighed significantly more than lean animals of either genotype, demonstrating no effect of *Odc1* on obesity (Fig. S3J). Orthotopic E0771 breast tumors in obese animals were larger than those in the lean animals, but there was no significant difference in tumor volume between Adipo-*Odc1* KO and littermate control animals (Fig. S3K). These data indicate that in contrast to *Gatm,* adipocyte *Odc1* is dispensable for obesity-accelerated tumor growth.

Knockdown of creatine transporter (*Slc6a8*) in breast cancer cells attenuates tumor growth

Our findings suggest a model in which GATM upregulation in adipocytes promotes synthesis of creatine, which is then exported for uptake into breast cancer cells to promote tumor progression. To test this model, we used *Slc6a8* KD or control cells in an orthotopic experiment in lean or obese mice (Fig. 3C). Obese animals were 60% heavier than lean ones, but there was no difference in body weight between obese animals that received control or *Slc6a8* KD cells (Fig. 3C). As we previously showed, *in vivo* tumor progression with control E0771 cells was significantly accelerated in obese compared to lean mice. However, obesity-accelerated tumor progression was abrogated with *Slc6a8* KD cells (Fig. 3D). At endpoint, *Slc6a8* KD tumors in obese animals were more than 50% smaller than obese control tumors (p=0.0005), and in fact were not different in volume than either lean group, in which there was no difference in progression between *Slc6a8* KD and control tumors (Fig. 3D). We also confirmed that *Slc6a8* mRNA expression was reduced in *Slc6a8* KD tumors compared to control tumors (Fig. 3E). To confirm the functional impact of *Slc6a8* silencing, we measured intratumoral creatine abundance using LC-MS and saw a 50% (p=0.009) reduction in creatine abundance in *Slc6a8* KD tumors compared to control tumors in obese mice (Fig. 3F). Taken together, these data confirm that cancer cell uptake of creatine is required for obesity-dependent tumor progression.

Transcriptomic analysis of cancer cells identifies *Acsbg1* as a driver of obesity-dependent tumor growth

To perform a comprehensive analysis of the interaction between adipose and breast cancer cells in the obese TME, we also profiled the transcriptomes of tumors from lean and obese animals. To enable specific isolation of cancer cells from heterogeneous tumors, we generated a stable mCherry expressing E0771 cell line (mE0771) and confirmed it retained the phenotype of *in vivo* obesity-accelerated tumor progression (Fig. S4A). We then utilized fluorescence-activated cell sorting (FACS) to isolate mE0771 cells from tumors in lean or obese animals for RNA-seq analysis (Fig. 4A). We identified a subset of genes that were consistently differentially regulated in obese cancer cells compared to lean, 10 of which are listed in Figure 4B. Of note, *Slc6a8* was one of the genes in this panel, with expression significantly upregulated in obese cancer cells compared to lean (p=0.004) (Fig. 4B).

One of the most differentially expressed transcripts in obese cancer cells was Acyl CoA synthetase Bubblegum Family member 1 (*Acsbg1*), with more than 13-fold increased expression compared to lean (p=0.0009) (Fig. 4B). We confirmed ACSBG1 overexpression in tumors isolated from obese animals via Western Blot (Fig. S4B). ACSBG1 converts long chain fatty acids to long chain fatty acyl CoAs (Steinberg et al., 2000; Mashek, Li and Coleman, 2007; Grevengoed, Klett and Coleman, 2014; Lopes-Marques et al., 2018). Long chain fatty acyl CoAs can participate in catabolic processes to produce ATP through oxidative phosphorylation or anabolic processes to produce fatty acid containing molecules, including phospholipids, triglycerides, and cholesterol esters (Fig. 4C).

To investigate the role of Acsbg1 in obesity-accelerated tumor progression, we produced a stable mE0771 cell line overexpressing *Acsbg1* (*Acsbg1* OE) or control LacZ (Fig. 4D) (Yang et al., 2011). *Acsbg1* overexpression does not have a cell autonomous effect on tumor cell proliferation (Fig. S4C). However, in orthotopic experiments, *Acsbg1* OE cells displayed significantly increased tumor progression in obese animals compared to control cells (Fig. 4E). There was no difference in body weight between obese animals that received *Acsbg1* OE or control cells (Fig. S4D). We confirmed ACSBG1 overexpression in bulk tumors isolated from each group by Western Blot (Fig. S4E). At endpoint, *Acsbg1* OE tumors in obese animals were 89% larger (p=0.0394) than control obese tumors. There were no differences between *Acsbg1* overexpressing and control tumors in lean animals, suggesting that *Acsbg1* in cancer cells, similar to *Gatm* in adipocytes, only promotes tumor growth in obesity.

To assess whether ACSBG1 is required for obesity-accelerated tumor progression, we produced mE0771 cells that stably express a short hairpin targeting *Acsbg1* (*Acsbg1* KD) and confirmed reduction of *Acsbg1* by RT-qPCR and Western Blot (Fig. S4 G and H). We implanted *Acsbg1* KD or control hairpin cells into obese and lean animals (Fig. S4F). Contrary to our prediction, *Acsbg1* KD tumors did not show attenuated progression *in vivo* compared to control tumors (Fig. 4F). However, ACSBG1 is a member of a family of long chain fatty acyl-coA synthetases, and increased activity of one or more of these other enzymes may compensate for the loss of *Acsbg1* expression in *Acsbg1*-silenced cells (Fig. S4I). We therefore repeated the previous experiment, but in addition to silencing *Acsbg1* in mCherry E0771 cells, we also administered triacsin C, a broad pharmacologic inhibitor of acyl coA synthetase activity (Tomoda et al., 1991; Mashima et al., 2009) (Fig. 4G), by intraperitoneal injection. This treatment did not cause significant weight loss or other signs of toxicity (Fig. S4J). Neither triacsin C nor *Acsbg1* KD alone significantly altered tumor progression, but combined *Acsbg1* KD with triacsin C treatment significantly attenuated tumor growth in obesity by 48% (p=0.0035) (Fig. 4H). There was no difference in tumor volume among any of the lean groups (Fig. 4I) These data indicate that long-chain acyl coA synthetase activity in cancer cells promotes tumor growth in the obese microenvironment.

Acsbg1-dependent tumor progression is supported by exogenous creatine

Our complementary transcriptomic approaches and *in vivo* genetic models show concomitant changes in peritumoral adipocytes and adjacent cancer cells that are closely linked to cellular energetics. On the one hand, upregulation of creatine biosynthesis in adipocytes and creatine uptake in cancer cells suggest increased capacitance for buffering the high-energy phosphate pool within cancer cells, as the canonical role of creatine is to interconvert with phosphocreatine in juxtaposition with ATP/ADP interconversion, a reaction mediated by creatine kinase. In parallel, cancer cells in the obese microenvironment upregulate *Acsbg1*, which has the capacity to expand the ATP pool by charging long-chain fatty acids in acyl-CoAs that can be processed through beta oxidation to generate ATP. However, the obese TME is also hypoxic (Fig. 1F), and thus beta-oxidation may not be readily accessible. Just as the Cr-PCr system in contracting muscle can replenish ATP when demand outpaces regeneration, it may be beneficial for cancer cells to have a similar buffering capacity to accommodate increased demand for ATP for anabolic processes of cell proliferation when oxidative phosphorylation is limited by hypoxia.

To test this hypothesis, we first asked whether *Slc6a8* expression is associated with ACSBG1 activity. We found by RT-qPCR that *Slc6a8* mRNA was significantly upregulated in obese, *Acsbg1* OE tumors compared to control (Fig. 5A). We next assessed whether *Acsbg1* OE cells have increased oxidative capacity and an expansion of the intracellular ATP pool. We used plate-based respirometry to measure oxygen consumption rates of *Acsbg1* OE and control cells and found that *Acsbg1* OE cells exhibited a 3.4-fold ($p<0.0001$) increased basal oxygen consumption rate relative to control cells (Fig. 5B, Fig. S5A). Notably, the proportion of basal respiration used to generate ATP through oxidative phosphorylation was substantially greater in *Acsbg1* OE cells than controls (Fig. 5B). In addition, *Acsbg1* OE cells displayed 1.9-fold ($p<0.0001$) increased maximal respiration (Fig. 5B, Fig. S5B). There were no differences in extracellular acidification rate (ECAR) between *Acsbg1* OE and control cells (Fig. S5C).

Using the Cell Titer Glo assay to quantify ATP *in vitro,* we found that *Acsbg1* OE cells had increased ATP content compared to controls (p=0.04) (Fig. S5D). This was confirmed on LC-MS measurement of the components of the creatine kinase/phosphocreatine circuit. We found that phosphocreatine and ATP were significantly more abundant in obese, *Acsbg1* OE tumors compared to controls (Fig. 5C). A targeted metabolomics screen for approximately 200 metabolites further corroborated this finding (Fig. 5C), with upregulation of all of the nucleotide triphosphates as well as phosphocreatine in *Acsbg1*-overexpressing tumors from obese animals. PCA of the entire sampled metabolome revealed that tumor *Acsbg1* overexpression remodels the cellular metabolic landscape only in obese hosts (Fig. 5D). The specific pathways that were perturbed were distinct between tumor *Acsbg1* overexpression in obese animals and the effect of obesity alone, as shown by pathway enrichment analysis using MBROLE (López-Ibáñez, Pazos and Chagoyen, 2016) (Fig. 5E). A heatmap plot of these perturbed pathways again revealed the differentiation between tumors from lean compared to obese animals (Fig. 5C), with *Acsbg1* overexpression showing a distinct pattern of upregulation of high-energy phosphate pools.

Finally, to test whether *Acsbg1*-dependent tumor progression is creatine-dependent, we generated *Acsbg1* OE E0771 cells that were deficient in *Slc6a8* and used these double-modified cells in an orthotopic experiment in lean or obese mice. After 9 weeks on HFD, all of the obese animals were significantly heavier than the lean animals, with no differences among obese groups (Fig. 6A). There were no differences in tumor volume among any of the groups in lean animals (Fig. 6B). As expected, *Acsbg1* OE cells produced tumors that were larger than control in obese mice; however, *Slc6a8*-deficient *Acsbg1* OE cells showed attenuated tumor growth (Fig. 6C). Therefore, these pathways appear to be functionally linked with ACSBG1-dependent tumor growth supported by creatine transport through SLC6A8.

SLC6A8 **and** ***ACSBG1*** **expression are associated with prognosis in patients with breast cancer**

Our studies revealed crucial roles for creatine metabolism and ACSBG1 activity in promoting worse tumor progression in a model of obesity-accelerated breast cancer. To assess the relevance of these findings to human breast cancer, we analyzed the mRNA expression of breast tumors from a previously published cohort of 405 patients with known BMI status and various tumor subtypes, including basal-like TNBC (Toro et al., 2016). We found that regardless of obesity status, *SLC6A8* and *ACSBG1* expression were significantly associated with worse tumor grade (Fig. 6D). Furthermore, among overweight and obese women, both *SLC6A8* and *ACSBG1* expression were associated with a basal subtype, which is associated with triplenegative status and portends a worse prognosis compared to Luminal A cancers (Fig. 6E).

Additionally, we utilized KM plotter, a microarray database that correlates tumor gene expression and relapse-free survival data from more than 6,000 breast cancer patients, to determine the prognostic value of *SLC6A8* and *ACSBG1* expression in breast cancer cells (Györffy et al., 2010). When limiting the search to TNBC, we found that high *SLC6A8* expression is associated with worse prognosis (Fig S6A and B). There was no significant association between *SLC6A8* or *ACSBG1* expression and prognosis in estrogen or progesterone receptor positive or Her2 amplified breast cancers. Together, these findings suggest *SLC6A8* and *ACSBG1* expression may be relevant for the prognosis of human disease.

Discussion:

Breast cancer affects 1 in 8 women in their lifetimes and leads to more than 40,000 deaths in the United States annually (Breast Cancer Statistics, 2019). Obesity is a major risk factor for both breast cancer incidence and worse disease prognosis, yet the mechanisms underlying these observations have not been fully elucidated. We hypothesized that crosstalk between adipose tissue and cancer cells in the TME may contribute to obesity-driven breast cancer progression. Using a murine model of obesity-accelerated breast cancer, we performed an integrative analysis of both peritumoral adipose tissue and neoplastic cells and identified a previously undescribed pathway whereby adipocyte creatine metabolism influences tumor progression, and strikingly, these effects appear to be obesity-specific and linked to the ability of cancer cells to charge fatty acids into acyl-CoAs.

As obesity results in a multitude of systemic and tissue-level changes that cannot be completely recapitulated *in vitro*, we utilized multiple *in vivo* models to dissect the relevance of this pathway to breast cancer progression. We demonstrate, via adipocyte-specific genetic deletion of *Gatm*, that adipocyte-derived creatine is critical for obesity-driven breast cancer progression. Interestingly, dietary creatine supplementation does not promote tumor growth in lean or obese animals, suggesting that creatine in the TME, not systemic creatine, plays an important role in promoting breast cancer progression in this model. Furthermore, cancer cells that do not express the creatine transporter show a complete ablation of obesity-accelerated tumor growth *in vivo,* establishing a requirement for exogenous creatine in promoting tumor growth in obesity. The implications of this creatine shuttle are suggested by our experiments demonstrating that *Acsbg1* is overexpressed by breast cancer cells in obese animals and that high *Acsbg1* expression promotes obesity driven tumor progression in a creatine-dependent manner *in vivo.* This dependence is associated with expansion of the high-energy phosphate pool in cancer cells, which may ultimately drive tumor progression through provision of the energetic requirements of cell proliferation. Together, these findings reveal a central role for creatine metabolism in promoting obesity-accelerated breast cancer progression.

Our data also shows that mRNA levels of *Slc27a4* are induced in breast cancer cells in obese mice. While SLC27A4 is a fatty acid transporter and acyl-CoA synthetase for very long chain fatty acids, it is not thought to be inhibited by triacsin C. Although *in vitro* data show that SLC27A4 can esterify long chain fatty acids (C16 or C18) in addition to very long chain fatty acids, it is unclear whether this activity occurs *in vivo* as *Slc27a4* null mice do not show defects in long chain fatty acid esterification (Hall et al., 2005). It is therefore likely that upregulation of *Slc27a4* in our obesity-accelerated breast cancer model represents a separate mechanism from the pathways we have targeted with *Asbg1* knockdown and triacsin C.

We propose a mechanism in which obese adipocytes undergo metabolic reprogramming in the presence of a tumor to enhance creatine production (Fig. 6F). The signals inducing this change are unknown and would be a rich area for future studies. Concurrently, cancer cells in the obese microenvironment upregulate ACSBG1, which promotes ATP production through oxidative phosphorylation as well as enhanced import of adipocyte-derived creatine from the TME through SLC6A8. Increased intracellular concentrations of both ATP and creatine support the production of phosphocreatine, which may promote tumor progression by ensuring a means to continue anabolic processes even during periods of tumor hypoxia. We have demonstrated with deuterated creatine experiments that cultured breast cancer cells can take up creatine to make phosphocreatine. While SLC6A8 has been proposed to transport both creatine and phosphocreatine, this has never been directly shown, and both adipocytes and cancer cells possess the machinery to convert creatine into phosphocreatine.

The creatine kinase/phosphocreatine circuit has well described roles in maintaining high levels of ATP during periods of increased energy demand, such as muscle contraction or rapid proliferation, and has been previously implicated in models of tumor progression, including HER2 positive breast cancer (Fenouille et al., 2017; Kurmi et al., 2018; Kazak and Cohen, 2020). Additional studies in another obesity-associated cancer, colorectal carcinoma, have revealed an essential role for the import of exogenous phosphocreatine through SLC6A8 to meet the high energy demands of metastatic colonization in the liver (Loo et al., 2015).

The relevance of these findings to human disease is corroborated by gene expression analysis from two human breast cancer cohorts. In overweight and obese patients, high *SLC6A8* and *ACSBG1* expression are associated with the more aggressive, triple negative basal subtype. Additionally, high expression of SLC6A8 and *ACSBG1* are associated with worse tumor grade, regardless of subtype, and *SLC6A8* expression is associated with worse prognosis in TNBC. These data support further investigation into the prognostic and therapeutic potential of targeting *SLC6A8* and *ACSBG1*, particularly in obese patients. Despite the recognized differences in outcomes between obese and non-obese patients, current standards of care offer the same treatments to both groups. The ability to customize treatment not only against tumor-specific molecular targets, but also for patient characteristics such as obesity would represent a significant advance in personalized medicine.

Advances in the detection and treatment of breast cancer have led to striking improvements in outcomes over the last several decades; however, breast cancer remains a major cause of morbidity and mortality worldwide. Furthermore, rapidly increasing rates of obesity, an established risk factor for worse breast cancer outcomes, threatens to undermine the progress made to improve the burden of this disease. Our work suggests that targeting creatine metabolism may be an appealing therapeutic strategy to mitigate the adverse effects of obesity on tumor progression in this vulnerable population of breast cancer patients. Moreover, the data presented here discover an essential role for creatine in facilitating obesity-dependent tumor growth and provide the basis for further studies investigating the role of creatine metabolism in other obesity-driven cancer types.

Limitations of Study

Since we were interested in studying both the tumor and the obese adipose microenvironment, we were limited to models compatible with animals susceptible to diet-induced obesity. All of the experiments were therefore conducted with the E0771 orthotopic model of breast cancer in B6 mice, which develop dietary obesity. While we present some limited evidence that our findings may be relevant to human disease, additional studies using “humanized” mouse models and well characterized patient cohorts will be crucial to establishing the role of creatine metabolism in human breast cancer. Our dietary studies supplying animals with exogenous creatine did not support tumor progression, and we believe this along with our genetic models reflects the importance of creatine in the TME. However, we were unable to directly trace adipocyte derived creatine into neighboring breast cancer cells in live animals. Future studies will seek to examine the tumor/adipose interface at cellular resolution and to develop *in vivo* stable isotope labeling approaches to trace the fate of metabolites from neighboring adipocytes into cancer cells in a cell type and region-specific manner. Such approaches will be necessary to further confirm our model and to more definitively link the creatine and ACSBG1 pathways. Furthermore, it is possible that creatine synthesis in other tissues and cell types beyond adipocytes may play a role in obesity accelerated tumor growth. This can be studied in the future by specifically deleting Gatm in other tissues.

STAR Methods

RESOURCE AVAILABILITY

Lead Contact—Further information and requests for resources and reagents should be directed to and will be fulfilled by the Lead Contact, Paul Cohen (pcohen@rockefeller.edu).

Materials Availability—All newly generated materials will be made available by the Lead Contact.

Data and Code Availability—The datasets generated during this study are available at The Gene Expression Omnibus. The adipose tissue RNA sequencing data is available at accession GSE165273. The cancer cell RNA sequencing data is available at GSE165275.

EXPERIMENTAL MODEL AND SUBJECT DETAILS

Cell Lines—All cells were cultured in RPMI 1640 medium (ThermoFisher) with 10% FBS and 1% Penicillin/Streptomycin at 37°C, 5% CO_2 unless otherwise noted. The E0771 cell line was purchased from CH3 BioSystems.

Animals: All animal studies were performed in accordance with the institutional guidelines of The Rockefeller University Institutional Animal Care and Use Committee (IACUC). Female C57Bl/6J wild-type mice were utilized for these studies and were purchased from Jackson Labs. Animals were maintained at The Rockefeller University Comparative Biosciences Center. Mice were 6-19 weeks of age for all experiments, and the ages of each cohort are noted in the corresponding figures. Unless otherwise specified, animals were group housed at 23°C and maintained in 12 hour light:dark cycles. *Gatm* floxed mice crossed to Adiponectin Cre (Adipo-Gatm KO) were provided by Dr. Bruce Spiegelman (Dana-Farber Cancer Institute) (Kazak et al., 2017). Rosa26^{fsTRAP} were purchased from Jackson Labs and crossed to Adiponectin cre mice (Zhou et al., 2013). *Odc1* floxed mice were generated using conventional gene recombination methodology in 129/SvEv x C57BL/6 FLP hybrid embryonic stem cells, which were then injected into C57BL/6 blastocysts (Ingenious Targeting Labs). LoxP sites were inserted such that exons 2-12 are deleted upon Cre-recombination. Adipocyte-specific *Odc1* knockout mice (Adipo-*Odc1* KO) were generated by crossing *Odc1* floxed mice to Adiponectin Cre mice.

METHOD DETAILS

Cell line modifications—The mCherry E0771 (mE0771) cell line was generated via lentivirus derived from pHIV-Luc-ZsGreen (provided by S. Tavazoie lab), and FACS was used to generate a bulk population of mCherry$^+$ cells. For knockdown studies, a short hairpin targeting *Slc6a8* (CTCAAGCCTGACTGGTCAAAG), *Acsbg1* (GCGCCTCAAAGAATTAATCAT), or scrambled control (GGCGCGATAGCGCTAATAATTT) was cloned into the pLKO.1 TRC cloning vector.

Lentivirus was produced by transfecting HEK-293T cells along with lentiviral packaging plasmids using Fugene transfection reagent (Promega). mE0771 cells were transduced with viral supernatant supplemented with 8 mg/mL polybrene. Puromycin (2ug/ml) was used to select shRNA or control expressing cells. For *Acsbg1* overexpressing cells, we obtained a pLX304-Blasticidin V5 vector encoding a V5-tagged Acsbg1 or LacZ protein from an ORF expression library *(22)*. Lentivirus was produced as above and *Acsbg1* or LacZ expressing mE0771 cells were selected with blasticidin at 50 ug/mL.

Mouse Diets—Lean mice were fed rodent chow diet (LabDiet 5053), *ad libitum.* For high fat feeding studies, animals were fed 60% fat diet, *ad libitum* (Research Diets, D12492) starting at 6 weeks of age for 9 weeks prior to tumor injections. Low fat diet (LFD) fed animals were fed 10% fat diet, *ad libitum* (Research Diets, D12450J). Body weights were measured every two weeks. For pair feeding studies, all animals were singly housed one week prior to starting the study and throughout the duration of the experiment. Daily caloric intake was measured, and pair fed-HFD animals were provided with HFD calorically matched to the average amount that LFD animals voluntarily consumed. Pair feeding was initiated one week before tumor injection and continued throughout tumor growth. For the creatine supplementation studies, animals were individually housed and fed *ad libitum* with the control or creatine-supplemented diet for one week prior to the study and throughout the duration of the experiment. The creatine supplemented diets were formulated to contain 2% creatine by weight.

Orthotopic injections and tumor measurements—Ovary intact, female mice were used for all orthotopic experiments. 50,000 E0771 cells were resuspended in 1:1 serum free RPMI 1640 medium and growth factor reduced, phenol red free Matrigel basement membrane matrix (Corning) and injected into the left 4th mammary fat pad of 15-week old mice using a 27g needle. Tumor volume was measured at the indicated time points starting at 6-7 days post tumor injection. The following formula was used to generate volume: Volume (mm^3) = 0.5 × length × ($width^2$), where length indicates the longest dimension and width is perpendicular to length. For *Gatm* KO experiments presented in Fig 2 K–M, data are pooled from two independent experiments (n=9-13 per group, per experiment). For *Slc6a8* KD experiments presented in Fig 3 C and D, data are pooled from two independent experiments *(experiment 1: HFD groups only n=9-11; experiment 2: all groups n=8).* For Adipo-Odc1 experiments presented in Fig S3, data are pooled from two independent experiments (experiment 1: n=11-15; experiment 2: n=12-14).

Body composition analysis—Body composition analysis was performed using an EchoMRI (Houston, TX) on the day of sacrifice.

RNA isolation, cDNA synthesis and qPCR—RNA was isolated from fresh or frozen tissue using Trizol (Invitrogen) and purified using RNAeasy columns (Qiagen). cDNA was synthesized using 1-2ug of RNA and the High Capacity cDNA Reverse Transcription Kit (Applied Biosciences). qPCR was performed using a QuantStudio 6 Flex Real-Time PCR System (Thermo Fisher Scientific). Power Sybr Green (Life Technologies) was used in a 384 well plate format. Relative gene expression difference was calculated using the DDCT method normalized to TBP or 18s. qPCR primers are provided in Table S1.

GFP-Translating ribosome affinity purification (TRAP)—Flash frozen mammary adipose tissue from Rosa26^{fsTRAP} transgene, adiponectin Cre positive mice was minced in 3ml of homogenization buffer (50mM Tris (pH 7.5), 100mM KCl, 12mM MgCl2, 1% NP40, 100ug/ml CHX, 1mg/ml heparin, 2mM DTT, 0.1u/μl RNAsin (Promega Madison, WI #N2115), 0.1 u/μl Superase (Thermo Fisher Scientific Waltham, MA #AM2696), and 1× Roche (Basel, Switzerland #11836170001) protease inhibitor. Tissue was further processed with a KONTES dounce tissue grinder (VWR 7ml Radnor, PA #KT885300-0007) 20 times with piston A and 20 times with piston B. Samples were then spun at 13k RPM for 10 minutes at 4°C. The lipid layer was removed, and supernatant was placed in a 5 ml tube and incubated with 4μl (5mg/ml) of ab290 to GFP (Abcam Cambridge, UK) for 1 hour at 4°C. 1750μl was saved for input. Protein G Dynabeads beads (Themo Fisher Scientific #10003D) were prepared by washing twice in low salt buffer (50mM Tris (pH 7.5), 100mM KCl, 12mM MgCl2, 1% NP40, 100ug/ml CHX, 2mM DTT). Antibody containing supernatant was added to 200μl of dry beads and incubated for 30min on a rotator at 4°C. Beads were washed with high salt buffer three times (50mM Tris (pH 7.5), 300mM KCl, 12mM MgCl2, 1% NP40, 100ug/ml CHX, 2mM DTT). RLT buffer (RNAeasy Qiagen #74106) was used to elute RNA from the beads. RNA was isolated using an RNAeasy micro kit (Qiagen #74034) and eluted in 14μl of water. cDNA was synthesized as described above.

RNA sequencing—RNA was isolated as above. For adipose samples, RNA was pooled from two animals per sample. RNA integrity number (RIN) was measured with a bioanalyzer (Aglient) and sequenced using the Illumina HiSeq 2500 at the Rockefeller Genomics Resource Center. Reads were mapped to the mm10 genome using TopHat and analyzed using DESeq. KEGG metabolic pathway analysis was performed using the GAGE method (Luo et al., 2009).

Fluorescence activated cell sorting—Fluorescence Activated Cell Sorting (FACS) was performed by the Rockefeller Flow Cytometry Resource Center. Tumors were harvested and digested using the Mouse Tumor Dissociation Kit (Miltenyi) according to the manufacturer’s instructions. Cells were stained with DAPI, resuspended in FACS buffer (PBS, 1% BSA, 0.1% HEPES pH= 7.4) and then sorted.

Metabolite measurements—Relative amounts of creatine, phosphocreatine, ATP and ADP were measured using LC/MS from snap frozen tissue. 100ug tumor was homogenized in the tissue lyser homogenizer (Qiagen) in cold 2:1 LC/MS grade methanol:LC/MS grade water, in pre-filled bead mill tubes (Fisher scientific). Polar metabolites were isolated using cold LC/MS grade chloroform containing 50mM Metabolomics Amino Acid Standard (Cambridge Isotope Labs). The polar phase was collected, nitrogen – dried, and stored at −80°C until use. Targeted polar metabolomics was performed by The Rockefeller University Proteomics Resource Center.

d3-Creatine tracing—0.8×10^6 E0771 cells were seeded in 6 cm plates 24hrs prior to adding labeled creatine. Cells were then supplemented with 200 μM [methyl-d3] creatine (Cambridge Isotope Laboratories, DLM-1302) in DMEM with dialyzed FBS for 4 hours. Cells were washed with 150 mM ammonium formate, followed by lysis in 0.38 mL of methanol/HPLC-grade water (50:50 (v/v)), 0.22 mL of ice-cold acetonitrile (ACN) (at −20 °C or colder) and six 1.4 mm ceramic beads. The mixture was homogenized in a bead beater (Qiagen TissueLyser) for 6 min at 20 Hz. Next, 0.6 mL of ice-cold dichloromethane and 0.3 mL of ice-cold HPLC-grade water were added. The samples were vortexed for 1 min, incubated on ice for 10 min and centrifuged at 4000 rpm for 10 min at 1°C. Water-soluble metabolites in the upper polar phase were collected and dried using a chilled vacuum centrifuge operating at a sample temperature of 4°C (Labconco). Samples were resuspended in 50 µl of HPLC-grade water before LC–MS analysis. Metabolites were profiled at the Rosalind and Morris Goodman Cancer Research Centre Metabolomics Core Facility by LC-MS using an Agilent 6530 QTOF equipped with a 1290 UPLC (Agilent Santa Clara, CA). Compounds were chromatographically separated using a Scherzo SM-C18 column 3 µm, 3.0×150mm (Imtakt Corp, Japan). The gradient started at 100% mobile phase A (5 mM ammonium acetate in water) with a 5 min gradient to 100% B (200 mM ammonium acetate in 80% water / 20% ACN) at a flow rate of 0.4 ml/min. This was followed by a 5 min hold time at 100% mobile phase B and a subsequent re-equilibration time (6 min) before next injection. Eluting compounds were ionized using an Agilent dual jet stream electrospray ionization source operating in positive mode. The source was set with the following parameters: Gas temperature of 325°C, drying gas of 9 l/min, sheath gas temperature 400°C, Sheath gas flow of 12 l/min, nebulizer pressure of 45 psi capillary voltage of 4000 V, nozzle voltage of 500 V. Ion optics were set with a fragmentor of 140 V, skimmer of 65 V. To maintain the instrument resolution reference masses, 121.05083 from purine and 922.009798 from HP0921, were infused using the second nebulizer. Data were collected in scan mode (100 to 1600 m/z) and MS/MS mode using a collision energy of 10, 20 and 30 V. Accurate peak mass and retention times were compared to authentic standards and MS/MS. Data were collected on matched samples that were treated with unlabeled creatine to separate deuterium incorporation from interfering ions. Stable isotope tracer data were analyzed using MassHunter Profinder Software B.08.00 (Agilent Technologies), which includes matrix correction, or data were analyzed using area under the curve from MassHunter Quant (Agilent Technologies).

Subcellular fractionation—Subcellular fractionation was performed using differential centrifugation. Frozen samples were minced into small pieces and homogenized in fractionation buffer using a KONTES dounce tissue grinder 20 times with piston A and 20 times with piston B on ice (VWR). Fractionation buffer included 20mM HEPES pH 7.4, 10mM KCl, 2mM $MgCl_2$, 1mM EDTA, 1mM EGTA, 1mM DTT, 1× protease inhibitor

(Roche), 1× phosphostop (Roche). Homogenate was incubated on ice for 20 minutes and strained through a 100μm filter. Tubes were then centrifuged at 720×g for 5 minutes at 4°C, following which, the supernatant was spun again at 10,000×g for 5 minutes to isolate the mitochondrial pellet. Supernatant was transferred to a fresh tube and spun in an ultracentrifuge at 40,000rpm for 1 hour at 4°C, to isolate the membrane fraction. The resulting pellet containing the membrane fraction was resuspended in one pellet volume of Tris Buffered Saline buffer containing 0.1% SDS. Samples were then run for protein quantification (see immunoblot assays).

***In vitro* adipocyte isolation and differentiation—**Adipose tissue was dissected and mechanically minced and enzymatically digested with buffer containing 10 mg/mL Collagenase D (Roche), 2.4 mg/mL Dispase II (Roche) and $CaCl_2$ (10mM). The stromal vascular fraction was isolated and cultured in of F-12 Glutamax medium (Thermo Fisher Scientific) containing 10% Fetal Bovine Serum (Gemini Bioproducts) and 1% PenStrep (Thermo Fisher Scientific) on collagen coated plates (Corning). Pre-adipocytes were differentiated after the cells reached 100% confluence with adipocyte differentiation medium containing 0.5mM IBMX (0.5mM), 1uM dexamethasone, 850 μM insulin, and 1 μM rosiglitazone. On day two, medium was switched to insulin and rosiglitazone only. After day 4, medium containing insulin was replaced every other day. On day 7, adipocytes were fully differentiated. Adipocytes were maintained in 37°C incubators with 10% CO_2.

Immunoblot assays—A tissue lyser (Qiagen) was used to homogenize fat and tumor tissue with RIPA lysis buffer (150mM NaCl, 1% NP40, 0.5% Sodium deoxycholate (DOC), 0.1% SDS, 25mM Tris (pH 7.4), 1x protease inhibitor (Roche), 1x phosphostop (Roche)). Protein was quantified using Pierce BCA Protein Assay kit (Thermo Scientific). 30μg of cellular lysate was resolved on 4-20% BisTris gels (Bio-Rad) and transferred to PDVF membrane using standard techniques. Immunoblots were incubated with primary antibodies as indicated, and developed using Western Lightning Plus-ECL (PerkinElmer), and imaged in a Bio-Rad Gel Doc System. Quantification was performed using the Bio-rad Image Lab Software or imageJ.

Immunohistochemistry—Tumors were fixed in 10% neutral buffered formalin overnight at 4°C and transferred to 70% ethanol. Paraffin imbedding and sectioning was performed by the Memorial Sloan Kettering Cancer Center Laboratory of Comparative Pathology. The slides were deparaffinized with xylene and hydrated in 100%, 95%, 80%, 70% ethanol, and water. Antigen retrieval was performed using 10mM sodium citrate and 0.05% tween at 92°C. Endogenous peroxidase activity was quenched using 1% hydrogen peroxide. The slides were blocked with 5% donkey serum for 30 minutes and incubated with primary antibody at 1:200 dilution overnight at 4°C. The slides were then incubated with secondary antibody at 1:500 dilution for 1 hour at room temperature. The stain was revealed using 3,3-diaminobenzidine and hydrogen peroxide. Then slides were counterstained using hematoxylin before being dehydrated using increasing concentrations of ethanol and mounted with Permount (Fisher Scientific). The slides were imaged using the Rockefeller University Bioimaging Resource Center, and the images were processed using imageJ.

EdU incorporation—Two hours prior to sacrifice, animals were treated with 25 mg/kg EdU via intraperitoneal injection. Tumor sections were prepared and treated according to the immunohistochemistry protocol through antigen retrieval. EdU was detected using the Click-It EdU Alexa Fluor 647 Kit (Thermo fisher) followed by incubation with 100ng/mL DAPI for 10 minutes at room temperature. The slides were mounted with ProLong Gold mounting medium (Thermofisher). Alexa 647 and DAPI were imaged using the Rockefeller University Bioimaging Resource Center and the images were processed using imageJ.

Triacsin C administration—1g of lyophilized Triacsin C (Cayman Chemical) was dissolved in 1mL DMSO. The concentrated stock was then dissolved 20x in 0.9% NaCl and sterile filtered. Triacsin C or vehicle control was delivered to animals via intraperitoneal injection three times per week at a dose of 2mg/kg/week.

ATP quantification—5,000 E0771 cells were plated per well of a 96 well plate. After 16h, ATP content was measured using the Cell-Titer-Glo kit (Promega) according to the manufacturer’s instructions, and luminescence was quantified using a plate reader.

Oxygen consumption and extracellular acidification rate measurements: Oxygen consumption rate and extracellular acidification rates were measured using a 96 well format XF96 Extracellular Flux Analyzer (Seahorse Biosciences). 30,000 cells per well were plated 16h before the assay. Mitochondrial or glycolysis stress tests were performed according to the manufacturer’s instructions. Oxygen consumption rate or extracellular acidification rate was normalized by cell count staining using NucBlue Reagent (ThermoFisher).

Human tumor gene expression analysis—Gene expression (previously processed with Partek Genomics Suite 6.6) and clinical information for each sample was obtained from Gene Expression Omnibus, using the series matrix file of the GSE78958 dataset. Gene expression for each sample was quantile normalized for analysis. Gene expression level changes between groups were tested with one-way ANOVA, followed by post-hoc testing with Tukey’s honestly significant test. The p-values for each comparison were adjusted with a Bonferroni correction.

Cell proliferation assay—150,000 E0771 cells were plated into each well of a 6 well plate. At 24, 48, and 72 hours, they were counted using trypan blue exclusion and a countess II automatic cell counter.

QUANTIFICATION AND STATISTICAL ANALYSIS

Unless otherwise noted, graphs display mean values +/− standard error of the mean (SEM). The n number is indicated in the figure legends. Animal body weight and RT-qPCR data was analyzed via two-way ANOVA (two-factors four groups), one-way ANOVA (one-factor three or more groups), or t-test (one-factor two groups). For longitudinal tumor volume experiments, a linear mixed effects model for repeated measures was used to analyze data with fixed effects for group, time, and group-by-time interaction. An unstructured covariance matrix was used to model the changes in variances over unequally spaced measurements. A compound symmetry covariance matrix was used in one experiment (Figure 4F) with insufficient degrees of freedom to estimate separate variances and covariances. Post-hoc testing was performed between select groups of interest at the last time point of each experiment. Cube root transformation was applied to skewed tumor volume distributions prior to analysis and chosen over log transformation to deal with tumor volume measurements of 0 mm^3. Residual plots were examined to evaluate the validity of model assumptions. Data analysis was performed using Proc Mixed in SAS Studio version 3.8. For all analyses, * $p< 0.05$, ** $p<0.01$, *** $p<0.001$, ****$p<0.0001$.

Supplementary Material

Refer to Web version on PubMed Central for supplementary material.

Acknowledgments:

We thank J.M. Friedman, B. Hirschhorn, B.M. Spiegelman, and S. Tavazoie for feedback and discussions. O.A.M., S.K.S., D.J.K, and R.G.G. were supported by a Medical Scientist Training Program grant from the National Institute of General Medical Sciences of the National Institutes of Health under award number T32GM007739 to the Weill Cornell/Rockefeller/Sloan Kettering Tri-Institutional MD-PhD Program; L.E.T. and V.C were supported by the Tri-Institutional MD-PhD Gateways to the Laboratory Program; R.G.M. was supported by R01 DK060581 and R01 DK124096; P.M.S was supported by a Terry Fox New Frontiers Program Grant (251427-251690); L.K. was supported by a Canadian Institutes of Health Research Grant (PJT-159529) and by the Canadian Foundation for Innovation John R. Evans Leaders Fund (37919); P.C. was supported by Susan G. Komen (CCR16377602).

References:

Bastarrachea J et al. (1994). Obesity as an adverse prognostic factor for patients receiving adjuvant chemotherapy for breast cancer. Annals of Internal Medicine 120, 18–25. [PubMed: 8250452]

Bhaskaran K et al. (2014). Body-mass index and risk of 22 specific cancers: a population-based cohort study of 5·24 million UK adults. Lancet 384, 755–765. [PubMed: 25129328]

Breast Cancer Statistics | CDC (2019). Available at: https://www.cdc.gov/cancer/breast/statistics/index.htm.

Calle EE et al. (2003). Overweight, obesity, and mortality from cancer in a prospectively studied cohort of U.S. adults. The New England Journal of Medicine 348, 1625–1638. [PubMed: 12711737]

Fenouille N et al. (2017). The creatine kinase pathway is a metabolic vulnerability in EVI1-positive acute myeloid leukemia. Nature Medicine 23, 301–313.

Global BMI Mortality Collaboration, Angelantonio Di et al. (2016). Body-mass index and all-cause mortality: individual-participant-data meta-analysis of 239 prospective studies in four continents. Lancet 388, 776–786. [PubMed: 27423262]

Grevengoed TJ, Klett EL and Coleman RA (2014). Acyl-CoA Metabolism and Partitioning. Annual Review of Nutrition 34, 1–30.

Györffy B et al. (2010). An online survival analysis tool to rapidly assess the effect of 22,277 genes on breast cancer prognosis using microarray data of 1,809 patients. Breast Cancer Research and Treatment 123, 725–731. [PubMed: 20020197]

Hales CM et al. (2017). Prevalence of Obesity Among Adults and Youth: United States, 2015-2016. NCHS data brief 288,1–8. Available at: http://www.ncbi.nlm.nih.gov/pubmed/29155689.

Hall AM et al. (2005). Enzymatic properties of purified murine fatty acid transport protein 4 and analysis of Acyl-CoA synthetase activities in tissues from FATP4 null mice. Journal of Biological Chemistry 280, 11948–11954.

Hanahan D and Weinberg RA (2011). Hallmarks of cancer: The next generation. Cell 144, 646–674. [PubMed: 21376230]

Johnstone CN et al. (2015). Functional and molecular characterisation of EO771.LMB tumours, a new C57BL/6-mouse-derived model of spontaneously metastatic mammary cancer. Disease Models & Mechanisms 8, 237–251. [PubMed: 25633981]

Morris SM (2016).‘Arginine Metabolism Revisited. The Journal of Nutrition 146, 2579–2586.

Kazak L et al. (2017). Genetic Depletion of Adipocyte Creatine Metabolism Inhibits Diet-Induced Thermogenesis and Drives Obesity. Cell Metabolism 26, 660–671. [PubMed: 28844881]

Kazak L and Cohen P (2020). Creatine Metabolism: energy homeostasis and cancer biology. Nature Reviews Endocrinology 16, 421–436.

Kurmi K et al. (2018). Tyrosine Phosphorylation of Mitochondrial Creatine Kinase 1 Enhances a Druggable Tumor Energy Shuttle Pathway. Cell Metabolism 28, 833–847. [PubMed: 30174304]

Ligibel JA et al. (2014). American Society of Clinical Oncology position statement on obesity and cancer. Journal of Clinical Oncology: Official Journal of the American Society of Clinical Oncology 32, 3568–3574. [PubMed: 25273035]

Loo JM et al. (2015. Extracellular Metabolic Energetics Can Promote Cancer Progression. Cell 160, 393–406. [PubMed: 25601461]

Lopes-Marques M et al. (2018). Expansion, retention and loss in the Acyl-CoA synthetase “Bubblegum” (Acsbg) gene family in vertebrate history. Gene 664, 111–118. [PubMed: 29694909]

López-Ibáñez J, Pazos F and Chagoyen M (2016). MBROLE 2.0-functional enrichment of chemical compounds. Nucleic Acids Research 44, 201–204.

Luo W et al. (2009). GAGE: generally applicable gene set enrichment for pathway analysis. BMC Bioinformatics 10, 161. [PubMed: 19473525]

Mashek DG, Li LO and Coleman RA (2007). Long-chain acyl-CoA synthetases and fatty acid channeling. Future Lipidology 2, 465–476. [PubMed: 20354580]

Mashima T et al. (2009). Acyl-CoA synthetase as a cancer survival factor: Its inhibition enhances the efficacy of etoposide. Cancer Science 100, 1556–1562. [PubMed: 19459852]

Park J, Euhus DM and Scherer PE (2011). Paracrine and endocrine effects of adipose tissue on cancer development and progression. Endocrine Reviews 32, 550–570. [PubMed: 21642230]

Park J and Scherer PE (2012). Adipocyte-derived endotrophin promotes malignant tumor progression. Journal of Clinical Investigation 122, 4243–4256.

Perry RJ and Shulman GI (2020). Mechanistic Links between Obesity, Insulin, and Cancer. Trends in Cancer 6, 75–78. [PubMed: 32061306]

Phang JM et al. (2015). Proline metabolism and cancer: Emerging links to glutamine and collagen. Current Opinion in Clinical Nutrition and Metabolic Care 18, 71–77. [PubMed: 25474014]

Quail DF and Dannenberg AJ (2019). The obese adipose tissue microenvironment in cancer development and progression. Nature Reviews Endocrinology 15,139–154.

Reeves GK et al. (2007). Cancer incidence and mortality in relation to body mass index in the Million Women Study: cohort study. BMJ 335, 1134–1139. [PubMed: 17986716]

Renehan AG et al. (2008).‘Body-mass index and incidence of cancer: a systematic review and meta-analysis of prospective observational studies. The Lancet, 371, 569–578.

Steinberg SJ et al. (2000). Very long-chain acyl-CoA synthetases: Human “bubblegum” represents a new family of proteins capable of activating very long-chain fatty acids. Journal of Biological Chemistry 275, 35162–35169.

Tomoda H et al. (1991). Evidence for an essential role of long chain acyl-CoA synthetase in animal cell proliferation: Inhibition of long chain acyl-CoA synthetase by triacsins caused inhibition of Raji cell proliferation. Journal of Biological Chemistry 266, 4214–4219.

Toro AL et al. (2016). Effect of obesity on molecular characteristics of invasive breast tumors: Gene expression analysis in a large cohort of female patients. BMC Obesity 3,. 1–9. [PubMed: 26793316]

Yang Xiaoping et al. (2011). A public genome-scale lentiviral expression library of human ORFs. Nature Methods 8, 659–661. [PubMed: 21706014]

Zhou P et al. (2013). Interrogating translational efficiency and lineage-specific transcriptomes using ribosome affinity purification. Proceedings of the National Academy of Sciences of the United States of America 110, 15395–15400. [PubMed: 24003143]

Highlights (phrases cannot exceed 85 characters including spaces)

- Gatm in peritumoral adipocytes promotes breast cancer progression in obesity.
- Acsbg1 in breast cancer cells promotes breast cancer progression in obesity.
- Creatine is a metabolite linking these pathways in obesity-dependent tumor growth.
- Acsbg1 and Gatm in breast cancer patients are linked to disease grade and outcome.

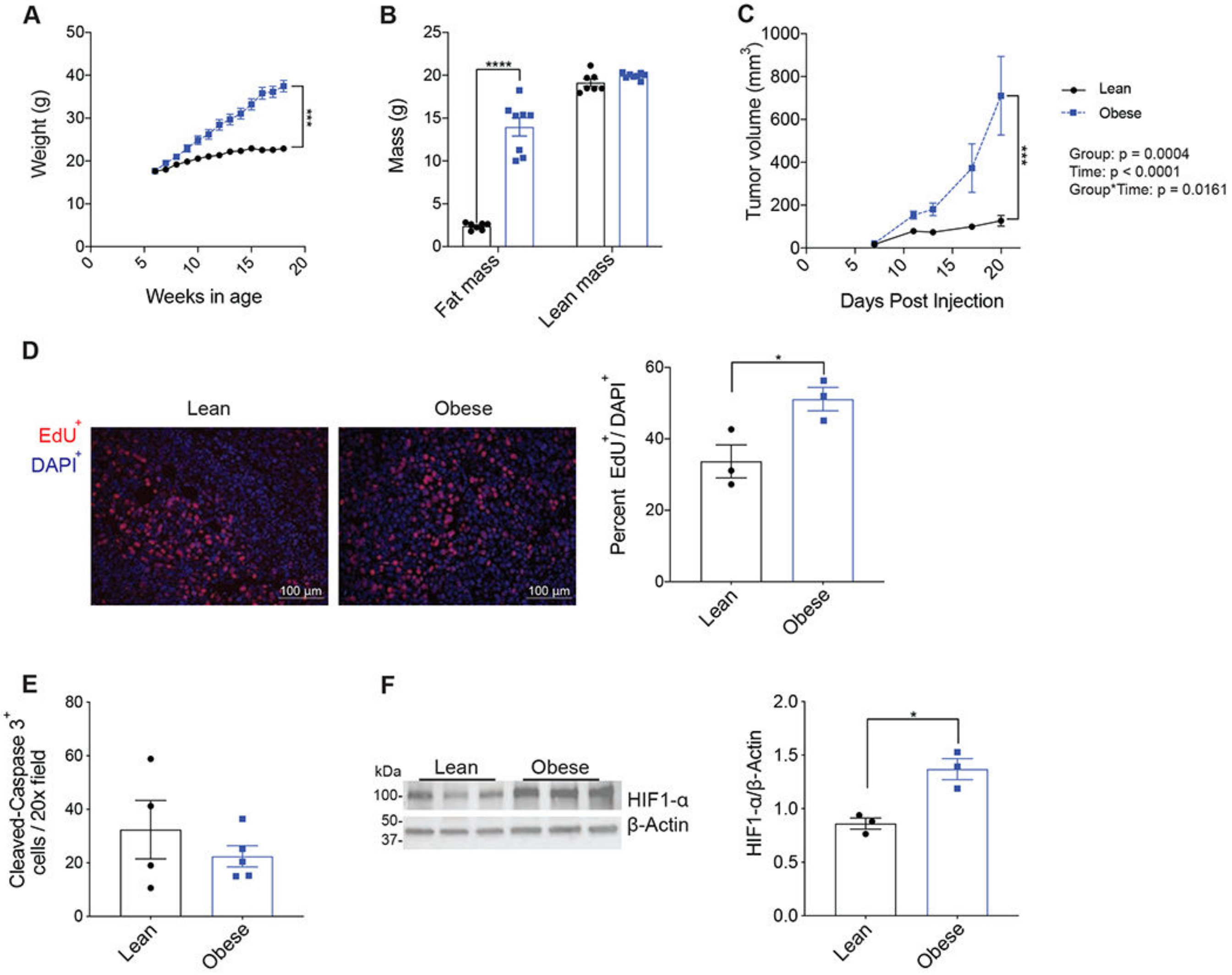

Fig. 1. Diet-induced obesity promotes tumor progression in an orthotopic breast cancer model

A. Body weight of female mice on chow or HFD (n=11 per group). B. Lean and fat mass of chow and HFD mice at necropsy (n=7-8 per group) from a separate, matched cohort. C. Longitudinal volume of orthotopic E0771 tumors in chow and HFD fed mice (n=11 per group). D. Representative image of EdU (red) and DAPI (blue) labeled tumor slides. Quantification of EdU$^+$ as a percentage of DAPI nuclei per 20x field (n=3 tumors per group). E. Quantification of cleaved caspase 3 positive cells per 20x field by immunohistochemistry (n= 4-5 tumors per group). F. Immunoblot of lysates from lean or obese tumors. HIF1α protein levels were normalized to β-actin and quantified using ImageJ. Data represent mean +/− standard error of the mean (SEM). * $p<0.05$, *** $p<0.001$, **** $p<0.0001$ For panel C, group, time, and group by time p-values are denoted and *** $p<0.001$ by post-hoc analysis at the final time point. See also Figure S1.

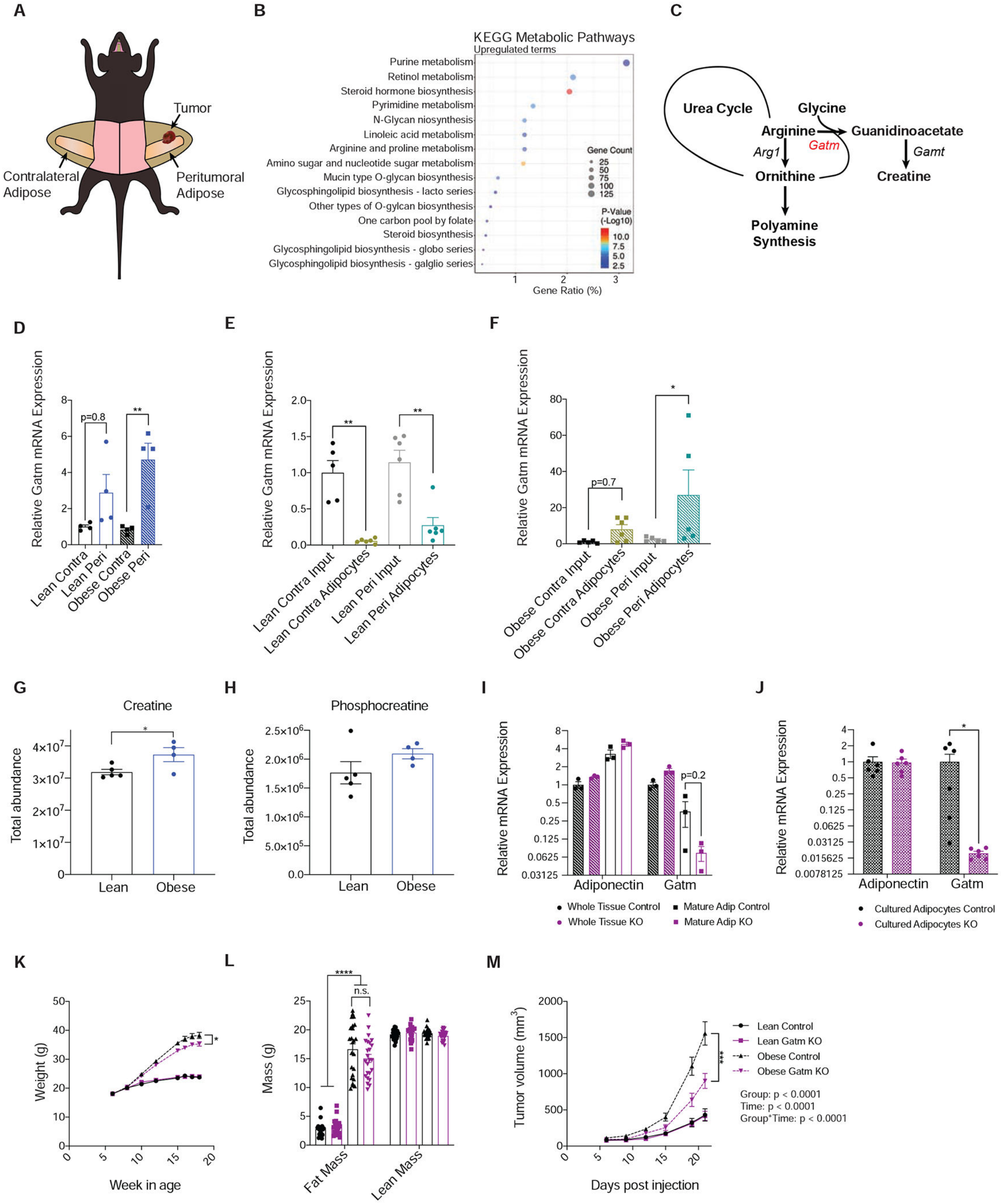

Fig. 2. Transcriptomic analysis of adipose tissue from obesity-accelerated breast cancer model

A. Diagram of orthotopic tumor location in mammary fat pad (peritumoral) and contralateral fat pad. B. KEGG metabolic pathway analysis of genes differentially expressed between HFD contralateral and peritumoral adipose tissue (n=4 per group). C. Segment of the Arginine and Proline Metabolism KEGG pathway demonstrating the creatine synthesis pathway. D. Relative mRNA expression of *Gatm* in bulk adipose tissue (n=4 per group). E. Normalized expression of *Gatm* in lean bulk tissue or adipocyte-specific TRAP purified mRNA (n=5-6 per group). F. Normalized expression of *Gatm* in obese bulk tissue (input) or adipocyte-specific TRAP purified mRNA (n=5-6 per group). G. Total abundance of creatine in bulk tumor from lean and obese mice by LC/MS. H. Total abundance of phosphocreatine in bulk tumor from lean and obese mice by LC/MS. I. Relative expression of Adiponectin and *Gatm* in whole adipose tissue or the mature adipocyte fraction (n=3 per group). J. Relative expression of Adiponectin and *Gatm* in cultured adipocytes differentiated from stromal vascular fraction (n=6 wells of differentiated adipocytes). K. Body weight of control or Adipo-*Gatm* KO mice on chow or HFD. L. Fat and lean mass of control or Adipo-*Gatm* KO mice at endpoint. M. Longitudinal volume of orthotopic E0771 tumors in lean or obese control or Adipo-Gatm KO mice. L-M; pooled from two independent experiments (n=20-27 per group). Data represent mean +/− SEM. *p<0.05, **p<0.01, *** p<0.001, ****p<0.0001. For panel M, group, time, and group by time p-values are denoted and *** p<0.001 by post-hoc analysis at the final time point. See also Figure S2 and S3.

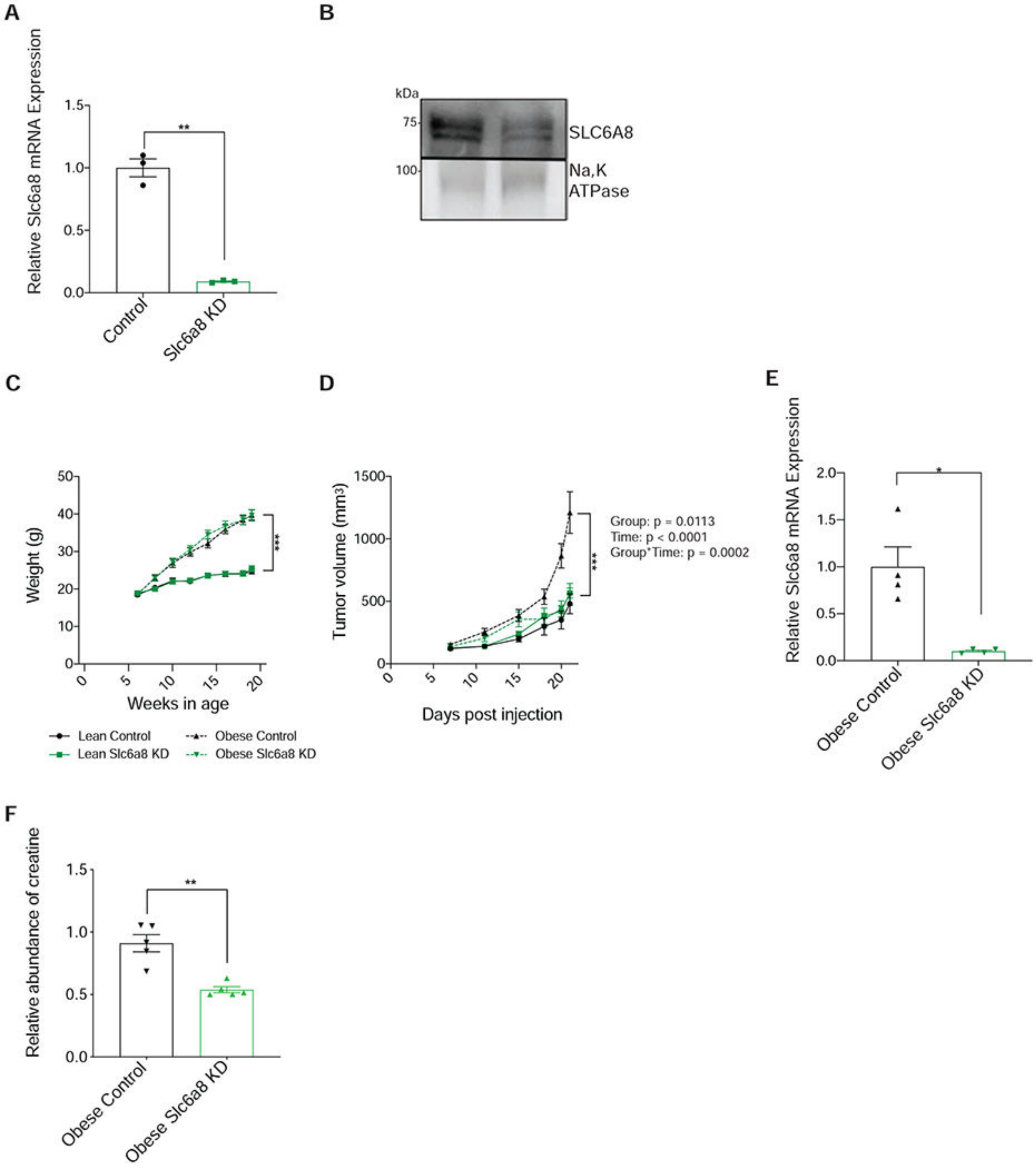

Fig 3. Genetic knockdown of creatine transporter (Slc6a8) in breast cancer cells attenuates tumor growth in obesity

A. Normalized mRNA expression of *Slc6a8* in control or *Slc6a8* KD cells. B. Immunoblot of Slc6a8 in membrane fractions of control (lane 1) or *Slc6a8* KD cells (lane 2). C. Body weight of B6 mice on chow or HFD (n=10-19 per group). D. Longitudinal volume of control or *Slc6a8* KD tumors in lean or obese mice (n=10-19 per group). E. Normalized expression of *Slc6a8* in bulk control or Slc6a8 KD tumors. F. Relative abundance of creatine as measured by LC/MS (n=5 per group). Data represent mean +/− SEM. *p<0.05, **p<0.01,

*** p<0.001, ***p<0.0001. For panel D, group, time, and group by time p-values are denoted in the figure and *** p<0.001 by pairwise post-hoc analysis at the final time point.

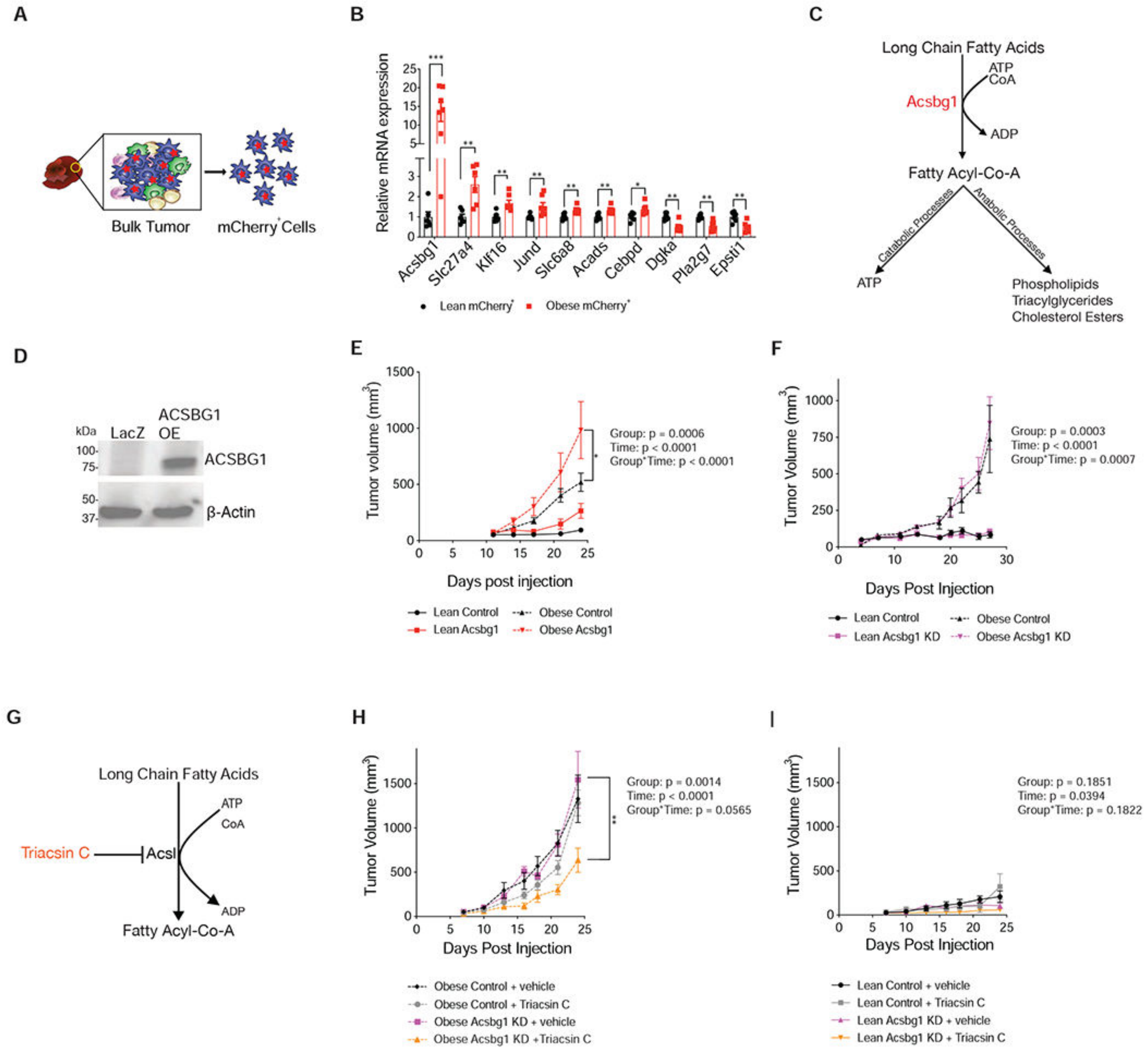

Fig 4. Transcriptomic analysis of cancer cells isolated from lean and obese tumors

A. Schematic depicting FACS to isolate mE0771 cells from bulk tumor. B. Relative expression of a panel of genes differentially regulated in obese mE0771 cells. C. Diagram depicting the role of Acsbg1. D. Immunoblot of control or *Acsbg1* OE cells. E. Longitudinal volume of control or *Acsbg1* OE tumors in lean or obese animals (n=9-12 per group). F. Longitudinal volume of control or *Acsbg1* KD tumors in lean or obese animals (n=8-10 per group). G. Diagram depicting the function of triacsin C. H. Tumor progression in obese animals with control or *Acsbg1* KD tumors, treated with vehicle or triacsin C (n=3-4 per group). I. Tumor progression in lean animals with control or *Acsbg1* KD tumors, treated with vehicle or triacsin C (n=4-7 per group). Data represent mean +/− SEM. *p<0.05, **p<0.01, *** p<0.001. For panels, E, F, H, and I, group, time, and group by time p-values are denoted in the figure. *p<0.05, **p<0.01 by post-hoc analysis at the final time point. See also Figure S4.

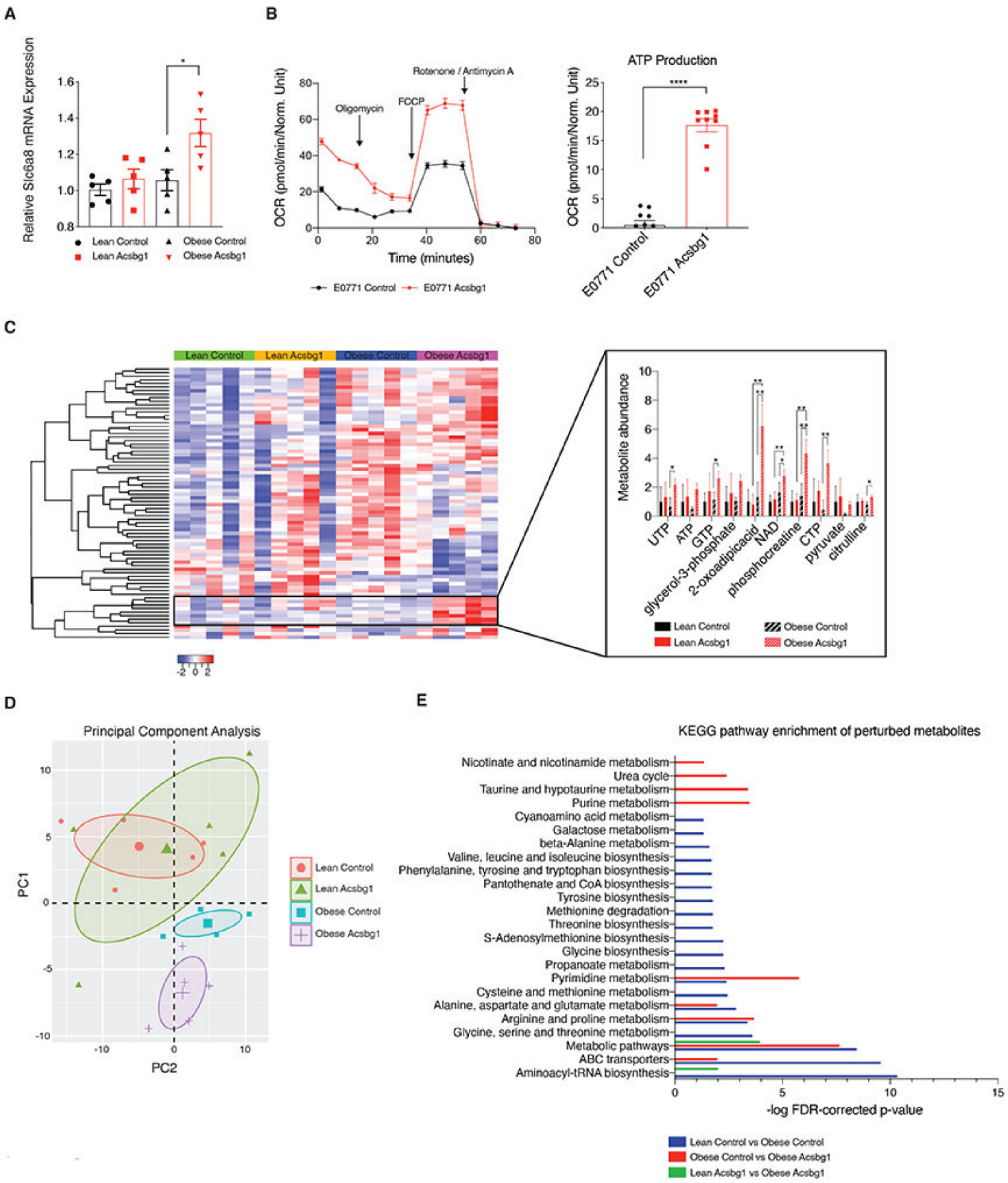

Fig 5. *Acsbg1*-overexpressing tumors in obese mice have remodeled metabolism

A. Relative mRNA expression of *Slc6a8* in bulk control or *Acsbg1* OE tumors in lean or obese animals (n=5 per group). B. Relative oxygen consumption rate of control or *Acsbg1* OE cells at baseline and following treatment with oligomycin, FCCP, and rotenone/antimycin. To the right is quantification of ATP generated through oxidative phosphorylation. C. Heatmap of dysregulated polar metabolites extracted from control or *Acsbg1* OE tumors from lean or obese mice. D. PCA plot of C. E. Significantly dysregulated (p-value < 0.05, student's t-test) metabolites from pairwise comparisons as labeled were queried against the KEGG database using MBROLE(López-Ibáñnez, Pazos and Chagoyen, 2016). Data represent mean +/− SEM. *p<0.05, **p<0.01, and ****p<0.0001. See also Figure S5.

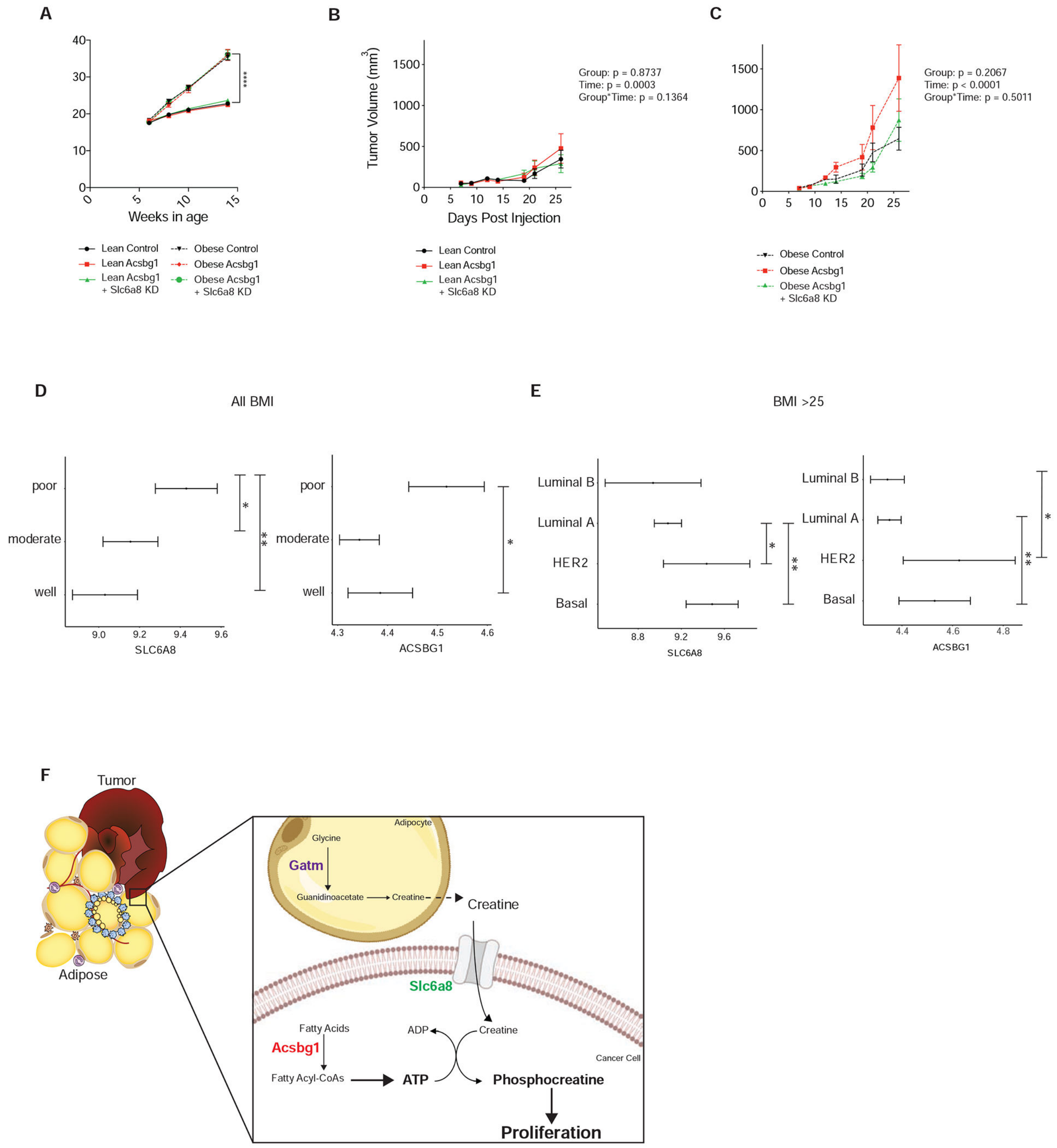

Fig 6. *Acsbg1-dependent* tumor progression is supported by exogenous creatine

A. Body weight of lean and obese control, *Acsbg1* OE, or *Acsbg1* OE + *Slc6a8* KD animals B. Longitudinal volume of control, *Acsbg1* OE, or *Acsbg1* OE + *Slc6a8* KD tumors in lean animals (n=8-9 per group) C. Longitudinal volume of control, *Acsbg1* OE, or *Acsbg1* OE + *Slc6a8* KD tumors in obese animals (n=5-7 per group). D. *SLC6A8* or *ACSBG1* expression in human breast tumors by grade of tumor differentiation (well, n=88; moderate, n=156; poor, n=178). E. *SLC6A8* or *ACSBG1* expression in human breast tumors by tumor subtype in overweight or obese women (Luminal A, n=141; Luminal B, n=26; Her2, n=33; Basal, n=68). F. Schematic depicting proposed mechanism. Data in A-C represent mean +/− SEM. Group, time, and group by time p values are denoted. Data in D and E represents normalized intensity (log2). The bar represents the 95% confidence interval of gene expression. The dot represents average expression level. * represent p value < 0.05; ** represent p value < 0.01. See also Figure S6.

KEY RESOURCES TABLE

REAGENT or RESOURCE	**SOURCE**	**IDENTIFIER**
Antibodies		
Anti-GFP	Abcam	Cat# AB290, RRID:AB_303395
Anti-Actin	Gene-Tex	Cat# 109639, RRID:AB_1949572
Anti-Slc6a8	Thermofisher	Cat# PA5-37060, RRID:AB_2553888
Anti-Na/K ATPase	Cell Signalling	Cat# 3010S, RRID:AB_2060983
Anti-Acsbg1	Thermofisher	Cat# MA5-25104, RRID:AB_2722807
Anti-Hif-1a	Cell Signalling	Cat# 36169T, RRID:AB_2799095
Anti-Cleaved Caspase 3	Cell Signalling	Cat# 9664, RRID:AB_2070042
Chemicals, Peptides, and Recombinant Proteins		
Triacsin C	Cayman Chemical	Cat#10007448
Puromycin	ThermoFisher	Cat#A1113803
Blasticidin	Sigma	Cat#15205-25MG
Trizol	ThermoFisher	Cat#15596026
Power Sybr Green	Life Technologies	Cat#4368708
Superase	ThermoFisher	Cat#AM2696
RNAsin	Promega	Cat#N2115
Collagenase D	Roche	Cat#11088882001
Critical Commercial Assays		
Mouse Tumor Dissociation Kit	Miltenyi	Cat#130-096-730
Click-It EdU Alexa Fluor 647°	ThermoFisher	Cat#C10634
Cell-Titer-Glo	promega	Cat#G7570
Seahorse XF Cell Mito Stress Test Kit	Agilent	Cat#103015-100
cDNA reverse transcription kit	Applied Biosystems	Cat#4368813
Quantabio cDNA kit	VWR	Cat#101414-098
RNAmicro kit	Qiagen	Cat#74004
RNeasy°	Qiagen	Cat#74106
Ultra sensitive insulin elisa kit	CrystalChem	90080
Mouse glucose assay kit	CrystalChem	81692
Deposited Data		
Human obesity breast tumor data	Gene Expression Omnibus	GSE78958°
Adipose RNA sequencing data	Gene Expression Omnibus	GSE165273
Cancer Cell RNA sequencing data	Gene Expression Omnibus	GSE165275
Experimental Models: Cell Lines		
E0771	CH3 biosystems	Cat# 94A001
Experimental Models: Organisms/Strains		

REAGENT or RESOURCE	**SOURCE**	**IDENTIFIER**
Mouse: C57BL/6J	The Jackson Laboratory	Cat #000664, RRID:IMSR_JAX:000664
Mouse: Adipo-GATM KO	Spiegelman Laboratory, Dana-Farber Cancer Institute	
Mouse: ODC1 floxed	Mirmira Laboratory, The University of Chicago	
Mouse: B6.129S4-Gt(ROSA)26Sortm1$^{(CAG\text{-}EGFP/Rpl10a,\text{-}birA)Wtp}$/J	The Jackson Laboratory	Cat #022367, RRID:IMSR_JAX:022367
Mouse: B6;FVB-Tg(Adipoq-cre)1Evdr/J	The Jackson Laboratory	Cat #010803, RRID:IMSR_JAX:010803
Oligonucleotides		
QPCR primers sequences°	Table S1	
shRNA targeting sequence: Slc6a8: CTCAAGCCTGACTGGTCAAAG	The Broad institute°	
shRNA targeting sequence: Acsbg1 GCGCCTCAAAGAATTAATCAT	The Broad institute	
shRNA targeting sequence: non targeting control GGCGCGATAGCGCTAATAATTT	The Broad institute	
Recombinant DNA		
pLX304-Blasticidin V5°	Yang et al, 2011	
pLKO.1 TRC cloning vector	Addgene	Cat# 10878, RRID:Addgene_10878
Software and Algorithms		
Image J	Schneider et al., 2012	https://imagej.nih.gov/ij/
RStudio	RStudio Team (2015)	https://rstudio.com
Other		
HFD	Research Diets	Cat#D12492
LFD	Research Diets	Ca#D12450J
LFD with 2% Creatine	TestDiet	5AZK
LFD control	TestDiet	5008
HFD with 2% Creatine	TestDiet	9GPR
HFD control	TestDiet	58Y1
Matrigel, phenol red free	Corning	Cat#356231